Circulation: Arrhythmia and Electrophysiology

ORIGINAL ARTICLE

Spatial Accuracy of a Clinically Established Noninvasive Electrocardiographic Imaging System for the Detection of Focal Activation in an Intact Porcine Model

Stephan Hohmann, MD
Maryam E. Rettmann, PhD
Hiroki Konishi, MD, PhD
Anna Borenstein, BS
Songyun Wang, MBBS
Atsushi Suzuki, MD, PhD
Gregory J. Michalak, PhD
Kristi H. Monahan, RN
Kay D. Parker, CVT
L. Katie Newman, CVT
Douglas L. Packer, MD

BACKGROUND: Noninvasive electrocardiographic imaging (ECGi) is used clinically to map arrhythmias before ablation. Despite its clinical use, validation data regarding the accuracy of the system for the identification of arrhythmia foci is limited.

METHODS: Nine pigs underwent closed-chest placement of endocardial fiducial markers, computed tomography, and pacing in all cardiac chambers with ECGi acquisition. Pacing location was reconstructed from biplane fluoroscopy and registered to the computed tomography using the fiducials. A blinded investigator predicted the pacing location from the ECGi data, and the distance to the true pacing catheter tip location was calculated.

RESULTS: A total of 109 endocardial and 9 epicardial locations were paced in 9 pigs. ECGi predicted the correct chamber of origin in 85% of atrial and 92% of ventricular sites. Lateral locations were predicted in the correct chamber more often than septal locations (97% versus 79%, *P*=0.01). Absolute distances in space between the true and predicted pacing locations were 20.7 (13.8–25.6) mm (median and [first–third] quartile). Distances were not significantly different across cardiac chambers.

CONCLUSIONS: The ECGi system is able to correctly identify the chamber of origin for focal activation in the vast majority of cases. Determination of the true site of origin is possible with sufficient accuracy with consideration of these error estimates.

VISUAL OVERVIEW: A visual overview is available for this article.

Key Words: echocardiography ■ electrocardiography ■ electrophysiology ■ fluoroscopy ■ tomography

https://www.ahajournals.org/journal/circep

WHAT IS KNOWN?

- Electrocardiographic imaging is used clinically to map arrhythmias noninvasively.
- Spatial accuracy of electrocardiographic imaging to identify the origin of focal activation has not been investigated thoroughly to date.

WHAT THE STUDY ADDS?

- The clinically established electrocardiographic imaging system is able to localize the true origin of focal activation with a median error of 20.7 mm.
- No significant differences in accuracy were found between cardiac chambers.

Noninvasive electrocardiographic imaging (ECGi) has recently been introduced into clinical cardiac electrophysiology.[1–4] The technology seeks to reconstruct the cardiac electrograms from a set of body surface potentials through an approximate solution of the inverse problem of electrocardiography.[5] Different experimental setups have been extensively validated in ex vivo torso tank experiments[6–8] and intact animal studies,[9,10] but, despite its clinical adoption, a thorough in vivo study of the spatial accuracy for the currently used system is lacking. The existing validation data has usually been obtained through comparison between noninvasive ECGi mapping and invasive electroanatomic maps and has either been limited to the left atrium[11] or was performed in patients with a diverse range of structural heart disease.[12] Accuracy reported in these studies differed by an order of magnitude.[11,12]

Here, we report the validation of the clinically used ECGi system in an intact porcine model of paced focal activation in all 4 chambers. Determination of the true pacing site was aided by the prior implantation of radio-opaque intracardiac markers which enabled highly accurate registration of the pacing site from biplane fluoroscopy to the cardiac computed tomography (CT) volume.

METHODS

The data that support the findings of this study are available from the corresponding author on reasonable request.

Animal Handling

All animal procedures were approved by the Mayo Clinic Institutional Animal Care and Use Committee (approved protocols A11713 and A00002273) and were performed in accordance with the standards laid out in the *Guide for the Care and Use of Laboratory Animals* and *The UFAW Handbook on the Care and Management of Laboratory and Other Research Animals.*[13,14]

After being fasted overnight with access to ad lib water, domestic swine (*sus scrofa domesticus*) of either sex, body weight ≈50 kg, were anesthetized using Telazol (veterinary formulation of tiletamine and zolazepam, 4.4 mg/kg), ketamine (2.2 mg/kg) and xylazine (2.2 mg/kg), intubated, and placed on mandatory ventilation at 16 to 18 breaths per minute and tidal volume of 10 to 12 mL/kg. A deep plane of anesthesia was maintained using either isoflurane (1%–3% in air with FiO2 of 0.3–0.5; in the electrophysiology lab) or a continuous propofol drip (0.25–0.30 mg/kg per min; during transport to and from the CT suite and during the actual CT scan). Heart rate and transcutaneous oxygen saturation were continuously monitored. In addition, arterial blood pressure and body temperature as well as the ECG were monitored while the animal was in the electrophysiology lab. The animals were positioned on a heating pad and warmed fluid was administered perioperatively to assist in maintaining normal body temperature. At the end of the study, animals were euthanized through induction of ventricular fibrillation, followed by rapid exsanguination.

ECGi System

The ECGi system (CardioInsight, Medtronic Inc, Minneapolis, MN) integrates anatomic data from a cardiac CT scan and body surface potentials acquired through 252 electrodes embedded in a vest on the patient's torso. The vest is fitted to the torso, a cardiac CT is acquired, and the torso electrode positions as well as the epicardial surface of the atria and ventricles are segmented from the CT.

Body surface potentials from all 252 electrodes are continuously sampled at 1000 Hz, and specific beats are selected for further analysis. The software reconstructs virtual unipolar electrograms on the segmented epicardial surface for the selected beat which can then be used to display isopotential maps or activation sequences.

Preparation and Insertion of Fiducial Markers

The electrode vest was applied to the anesthetized animal. Electrode contact to the skin was verified using the ECGi system's display of signal quality and by additional inspection of tracings for noise. The animal was then positioned supine in an immobilizing vacuum cushion (BodyFIX BlueBAG; Elekta AB, Stockholm, Sweden) and transferred onto the fluoroscopy table (Artis zee biplane, Siemens, Forchheim, Germany). Vascular access was obtained using a cut-down technique in the external jugular vein and 12 Fr and 8 Fr hemostatic introducer sheaths (Cordis, Milpitas, CA) were inserted. A 10 Fr, 5.5 to 10 MHz intracardiac echocardiography catheter (Acuson AcuNav catheter and Acuson Sequoia ultrasound imaging platform, Siemens, Mountain View, CA) was placed in the right atrium via the external jugular vein. A 7 Fr decapolar electrophysiology catheter (Response, Abbott Laboratories, St Paul, MN) was placed in the coronary sinus and connected to a digital amplifying and recording system (CardioLab Electrophysiology Recording System, GE Healthcare, Marlborough, MA).

Introducer sheaths in the femoral artery (8 Fr) and vein (9 Fr) were placed by direct percutaneous access under ultrasound guidance. Invasive blood pressure monitoring was established using the femoral arterial sheath. A femoral vein introducer sheath was exchanged with an 8.5 Fr SL1 sheath

(Abbott Laboratories, St Paul, MN). Transseptal puncture was performed with a transseptal needle (BRK, Abbott) under intracardiac ultrasound guidance. After transseptal access had been obtained the SL1 sheath was exchanged for an 8.5 Fr steerable introducer (Agilis NxT, Abbott). Heparin was administered intravenously to maintain an activated clotting time greater than 250 seconds after transseptal puncture.

Angiograms of all cardiac chambers were performed using a 6 Fr angiography catheter and 20 mL contrast material per chamber (Omnipaque 350, GE Healthcare, Marlborough, MA). Radio-opaque clips (Quick Clip 2; Olympus, Shinjuku, Japan) designed for endoscopic clipping were then applied through the steerable introducer sheath and deployed in unique locations in all 4 cardiac chambers under fluoroscopic and ultrasound guidance to serve as fiducial markers.[15]

Computed Tomography

With the animal still under anesthesia, a cardiac gated CT scan (Somatom Definition Dual Source, Siemens, Forchheim, Germany) was performed soon after clip placement. Care was taken to include the entire electrode vest in the CT volume. Intravenous contrast material was administered and scan timing was aimed at homogeneous contrast filling of the right and left heart. Volumes for each of 10 phases of the cardiac cycle were reconstructed from a scan obtained during ventilator breath hold (0.4 mm slice thickness, field of view 300–400 mm [in-plane resolution 0.59–0.78 mm per pixel]). A diastolic phase volume was used for segmentation and further analysis.

Endocardial Pacing

Pacing at various sites in all 4 chambers was performed using a 3.5 mm tip 7.5 Fr electrophysiology catheter (Navistar Thermocool, Biosense Webster, Diamond Bar, CA) connected to a programmed stimulator (Micropace EPS320, GE Healthcare). Catheter placement was aided by the steerable sheath if necessary. Left sided structures were accessed via the transseptal puncture. Pacing output was set to 2.0 ms pulse width at just above the diastolic pacing threshold and was performed during free breathing. Biplane fluoroscopy sequences were acquired in breath hold at 15 frames per second immediately after each pacing train to document the catheter position at the time of pacing. The investigator determining the pacing location on the ECGi system was blinded to the catheter position.

Epicardial Pacing

In one animal, pericardial access was obtained using a sub-xiphoid approach and a Tuohy needle. After confirming access to the pericardial space, a 9F introducer sheath was placed over the wire, and pacing of the ventricular epicardium was performed following the same protocol as described for endocardial pacing.

Determination of True Pacing Location

Biplane fluoroscopy sequences were acquired for each pacing location. An end-diastolic frame was identified in each sequence. The catheter tip and each one of the fiducial marker clips were annotated and their 2D image pixel coordinates in both corresponding images recorded. Additional data pertinent to the respective fluoroscopy sequence (image intensifier physical pixel spacing, imager angulation, tube-to-detector distance and tube-to-isocenter distance) were read from the Digital Imaging and Communications in Medicine metadata stored in the image files. The positions of each fiducial marker and the catheter tip in 3-dimensional (3D) space were then geometrically reconstructed from their fluoroscopic image coordinates and this additional data. (Figure 1).

After identification of the fiducial marker positions in the CT volume, the entire set of fluoroscopy-derived fiducial marker positions was registered to their corresponding positions on CT images using a rigid (6 df) least squares fit registration. This registration was then applied to the fluoroscopy-derived catheter tip position as well.

Reconstructed pacing locations were classified according to the cardiac chamber and whether they were in a lateral or septal position. For this classification, septal included locations on the interventricular or interatrial septum and any paraseptal locations of the anterior or inferior ventricular wall (the central third in a left anterior oblique projection with cut lines parallel to the septum). All other locations were classified as lateral. Apical locations were also classified as lateral for this purpose.

Phantom-Validation of the Fluoroscopy-Based Localization Approach

The accuracy of this approach was validated using a static phantom with 7 radiopaque markers. Six different angulations of the biplane fluoroscopy were used, with the angle between both imagers ranging from 60° to 90°. Measurements were performed as described above, and the 3D coordinates for each marker were reconstructed from the fluoroscopy images. Errors were calculated by first registering the reconstructed point cloud to the real-world coordinates using 6 of the 7 reconstructed marker positions and then measuring the residual distance for the position not used in the registration.

Detection of the Pacing Location on ECGi and Error Measurement

Three paced beats per location were selected and their virtual unipolar electrograms reconstructed on the segmented surface. The pacing point was determined by an investigator blinded to the true pacing location (A. Borenstein) by analyzing the global activation pattern and the electrogram signals of the ensuing activation post pacing. If the earliest signal was found to occur simultaneously at multiple points in close vicinity, the centroid of this set of points was used. Absolute distances between the true pacing location and the predicted pacing location were calculated as Euclidean distances between the 2 points in space.

Computational Analysis and Statistical Methods

Data are reported as mean±SD or median (first quartile; third quartile), as appropriate. Statistical calculations were performed using R 3.5.1 (R Foundation for Statistical Computing, Vienna, Austria). Differences between 2 groups were evaluated using Student's *t* test if normality

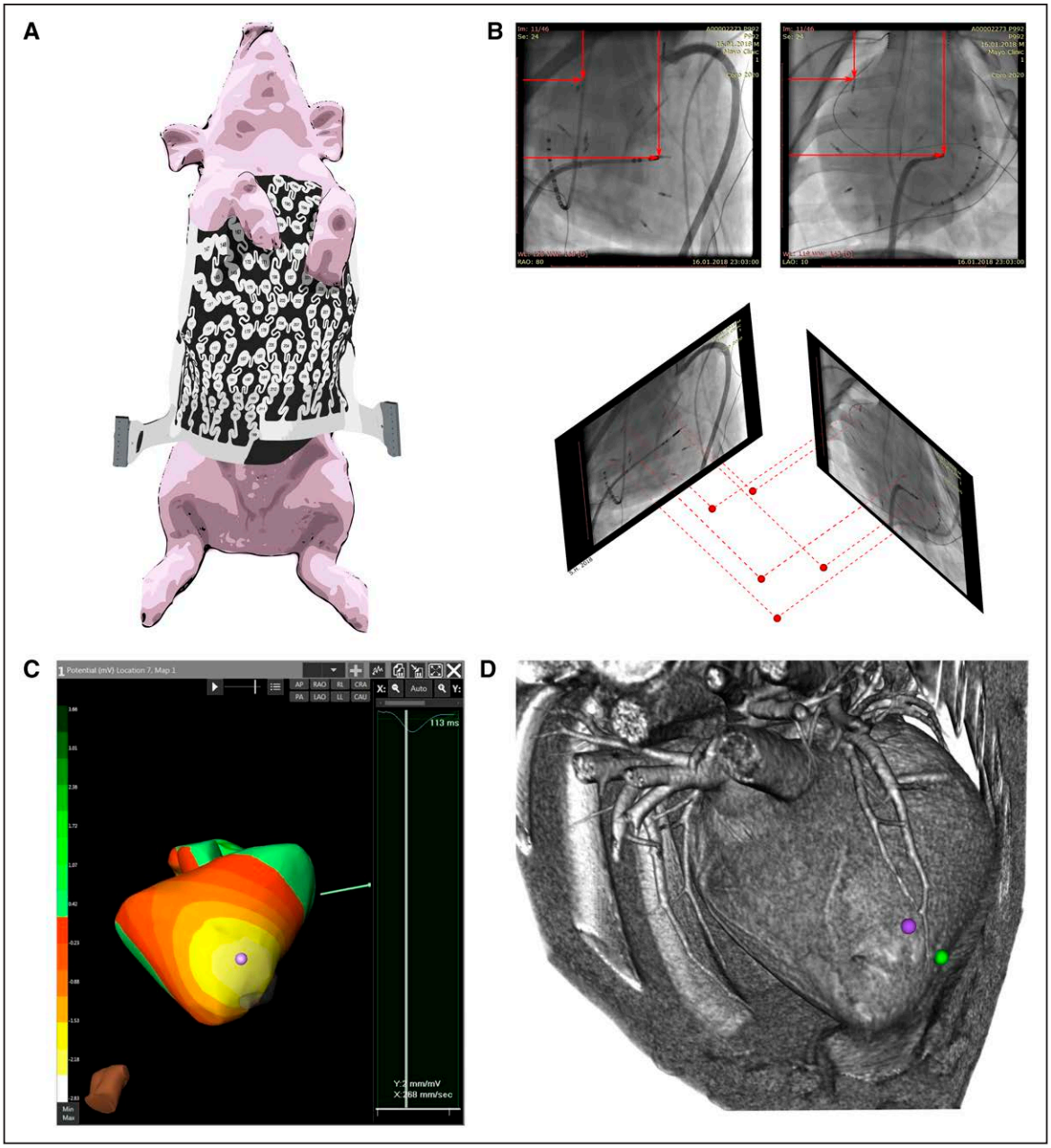

Figure 1. Study and analysis workflow.
A, Animal with ECG acquisition vest. **B**, Geometric reconstruction of fiducial marker and catheter tip positions in 3D from corresponding biplane fluoroscopy images. **Top**, Measurements of clip and catheter positions in a set of biplane fluoroscopy images. This is shown for one clip and the catheter tip only but was performed for all clips and the catheter tip. **Bottom**, Reconstruction of a 3D point cloud from biplane fluoroscopy images. Each point (red sphere) is located at the intersection of its two projection vectors shown as red dashed lines. **C**, Electrocardiographic imaging (ECGi) map. ECGi information represented as isopotential lines on the segmented ventricular surface, from −2.8 mV (white) to +3.66 mV (dark green). The location of the earliest negativity has been marked by the purple marker. **D**, Corresponding volume rendered computed tomography (CT), oriented in the same caudal right posterior oblique view as (**C**). The inferior aspect of the heart is shown. The purple marker corresponds to the purple marker in (**C**). The green marker identifies the true pacing location as reconstructed from fluoroscopy (near the RV apex). Euclidean distance between the 2 points in space was 17.9 mm in this case.

could be assumed, and using the Mann-Whitney *U* test in non-normal distributed data. For differences between more than two groups the Kruskal-Wallis rank sum was used. Frequencies were compared using Fisher's exact test. *P* values <0.05 were considered statistically significant in all statistical tests. Three-dimensional reconstruction from biplane fluoroscopy and all other nonstatistical numerical analyses were performed using the GNU Octave numerical computation suite (version 4.4.1, JW Eaton et al). Three-dimensional Slicer 4.10.0 was used to integrate the CT imaging and 3D model data, and for visualization purposes.[16]

RESULTS

Study Characteristics

ECGi validation studies were performed in 9 domestic pigs (4 of them male). The animals' median body weight

was 49.8 (49.0–51.4) kg. A total of 118 locations were paced (63 endocardial atrial, 46 endocardial ventricular, and 9 epicardial ventricular, see Table). One animal developed ventricular fibrillation during pacing and could not be defibrillated. Therefore, no left ventricular sites were available for analysis in this animal.

Validation of the Fluoroscopy-Based 3D Reconstruction

A phantom-validation of the fluoroscopy-based localization algorithm yielded a mean error of 1.56±0.63 mm (n=42 measurements). This demonstrates that fluoroscopy-based reconstruction of fiducial marker and catheter tip positions in 3D space is possible with sufficient accuracy.

Segmentation Surface Characteristics

One atrial and one ventricular epicardial surface were segmented from the diastolic phase cardiac CT in all animals using the ECGi software. Virtual unipolar electrograms were calculated for discrete points (vertices) on these surfaces. The median number of vertices defining the surface was 1503 (1485–1589) for the atrial and 1607 (1585–1620) for the ventricular segmentations, with 8.90 (8.56–10.78) and 6.57 (6.25–7.08) vertices per cm^2, respectively.

Chamber Prediction Accuracy

For 4 of 109 endocardial pacing locations, no location could be determined on the ECGi system due to excessive noise in the virtual unipolar electrograms. In the remaining 105 locations, the correct chamber (left or right) was identified in 39 of 46 (85%) ventricular pacing sites and in 54 of 59 (92%) atrial sites. No significant difference was found between atrial and ventricular prediction accuracy (P=0.35). The chamber prediction (left or right) was correct more often for lateral than for septal pacing locations, with 56 of 58 lateral locations (97%) and 37 of 47 septal locations (79%) predicted correctly (P=0.005)

Distances Between Paced and Predicted Site

The median distance between the true pacing location and the predicted location in all pacing locations was 20.7 (13.8–25.6) mm and was less than 36.6 mm in 90% of cases. Representative ECGi maps and the corresponding true pacing positions are shown in Figure 2. Distances for individual cardiac chambers are shown in Figure 3. Of note, no significant difference in the distributions of the distances was found among cardiac chambers (P=0.57, Kruskal-Wallis rank-sum test).

Impact of Distance to Segmented Surface

The ECGi signal was reconstructed on a segmentation of the epicardial surface obtained from the cardiac CT. However, the true pacing locations were located at varying distances from this surface. In free wall pacing locations, these distances were determined by the myocardial wall thickness and catheter-induced wall displacement. In septal locations the distance to the nearest epicardial surface played a larger role, with distances in ventricular septal locations ranging from 2.0 mm (inferior paraseptal location) to 21.9 mm (midseptal location).

The median distances between the pacing location and the nearest point on the segmentation surface were 2.97 (2.02–4.51) mm in the left atrium, 4.25 (2.40–6.02) mm in the right atrium, 8.17 (5.34–11.63) mm in the left ventricle (LV), 4.91 (3.62–6.78) mm in the right ventricle (RV), and 3.66 (2.51–3.77) mm for epicardial pacing locations.

Table. Overview of the Animal Studies

Study No.	Animal Sex	Animal Weight	No. of Paced Locations					
			LA	RA	LV	RV	EPI	Total
1	m	34.0 kg	6	3	0	2	0	11
2	f	47.0 kg	2	2	2	2	0	8
3	m	53.2 kg	3	1	2	2	0	8
4	m	49.0 kg	6	6	2	2	0	16
5	f	49.0 kg	6	6	6	6	0	24
6	m	51.4 kg	2	1	2	2	0	7
7	f	49.8 kg	2	3	2	1	0	8
8	f	51.0 kg	3	3	3	2	0	11
9	f	51.9 kg	3	5	4	4	9	25
Sum			33	30	23	23	9	118

EPI indicates epicardial; f, female; LA, left atrium; LV, left ventricle; m, male; RA, right atrium; and RV, right ventricle.

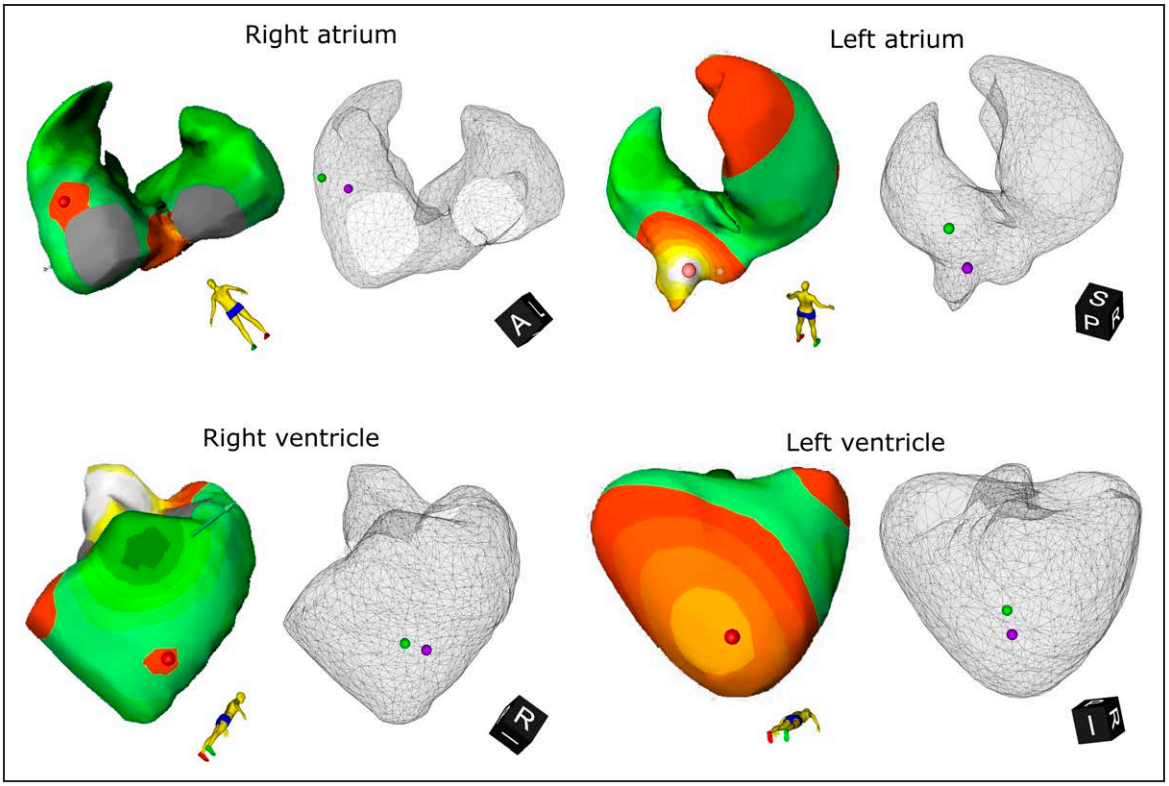

Figure 2. Representative electrocardiographic imaging (ECGi) maps (left) and corresponding reconstructions of the true pacing locations (right). **Left**, The ECGi maps show a still frame from the activation sequence animation at the time of the earliest negative epicardial potential, with red/orange/white indicating areas of negative potential at this given point in time and light to dark green indicating more positive potentials. The marker indicates the point identified as earliest location by the blinded investigator. **Right**, Surface as in the ECGi map in a similar view orientation. The purple marker dot corresponds to the earliest location on the ECGi map, and the green marker dot indicates the true pacing position.

No significant effect of the pacing location to surface distance on the measured error distance was found (*P*=0.16 for linear model).

Projection of Pacing Locations Onto the Segmented Surface

We performed a secondary analysis using the surface vertex closest to the true pacing position as reference location. A representative example for an LV pacing site is shown in Figure 4. The median distance between the surface projection of the true pacing location and the predicted location was 20.7 (12.5–28.5) mm, not different from the absolute distance measurements without the surface projection.

Comparison of Endocardial and Epicardial Pacing Locations

The epicardial pacing locations in one animal were located on the apical (n=2) and basal (n=2) RV free wall, the anterior RV outflow tract (n=1), the anterior LV (n=2) and the basal-lateral LV wall (n=2). The error distances observed in the 9 epicardial pacing locations (20.4 [10.5–24.0] mm) did not differ significantly from those observed for ventricular endocardial pacing locations in the same animal (18.9 [14.3–22.8] mm, *P*=0.88 versus epicardial) or for all endocardial pacings in all animals (21.0 [14.1–25.6] mm, *P*=0.43 versus epicardial).

Comparison of Different Analysis Techniques

The pacing locations were predicted as the virtual electrogram with the earliest negative potential. This was based on earlier experimental data showing an area of early epicardial negativity at the site of endocardial or epicardial pacing.[18] We also performed another analysis where the site of earliest epicardial activation (wave front breakthrough) was used to determine the pacing site. Both initial negativity analysis and epicardial breakthrough analysis used the ensuing global activation patterns and the electrogram signal morphologies to predict the pacing locations. The positional correlation between both analysis techniques was limited: Pacing locations predicted using either method differed by a mean distance of 16.6±13.8 mm from each other. However, when comparing the accuracy of both techniques against the true pacing locations, error distances were similar (median distance to true location of 21.2 [16.2–29.1] mm for the earliest activation breakthrough

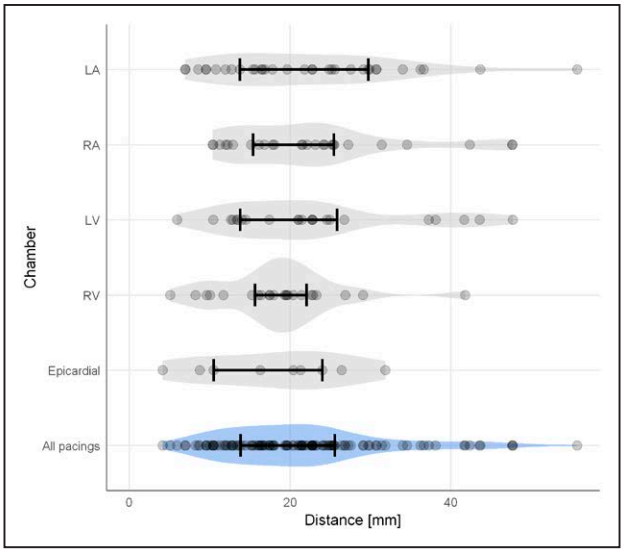

Figure 3. Distances between true pacing location and the location predicted by the electrocardiographic imaging (ECGi) system, per cardiac chamber and epicardially.
Each point indicates one data point. The error bars indicate the interquartile range. The light grey or blue violin plots[17] show the distribution density estimate. The plot at the bottom represents the aggregate of all pacings across all chambers. LA indicates left atrium; LV, left ventricle; RA, right atrium; and RV, right ventricle.

sites versus 20.7 [13.8–25.6] mm for the earliest negativity approach, *P*=0.19)

Pacing Output

Bipolar pacing was performed at 2 ms pulse width and with a current just above the diastolic threshold. However, pacing thresholds varied widely at different pacing locations and pacing output thus ranged from 0.4 to 10.0 mA. We, therefore, dichotomized the pacing locations according to the applied pacing output current below or above the median of all outputs and compared the error distances in both sets. In the low-output set, the mean pacing current was 1.13±0.42 mA, and the mean distance between true and predicted pacing site was 23.3±10.4 mm. In the high-output set, the mean pacing current was 4.22±2.04 mA, and the mean distance was 20.1±10.1 mm (difference not significant, *P*=0.10). Likewise, in a linear model of distance versus pacing output no significant effect of the pacing output was found (*P*=0.08 for model). Based on this finding, we concluded that the pacing output did not confound the measured accuracy in our model.

DISCUSSION

The main findings of the present study are (1) ECGi detects pacing locations at a median distance of 20.7 mm from the true pacing site. (2) No significant difference in precision was found between the different cardiac chambers. (3) The identification of the chamber of origin is significantly more often correct for lateral than for septal foci.

Previous Validation Attempts of ECGi

Since experimental ECGi systems were first described in the early 1990s,[6] determination of their accuracy has been of great interest, but in vivo validation has been fraught with difficulties. A major challenge has

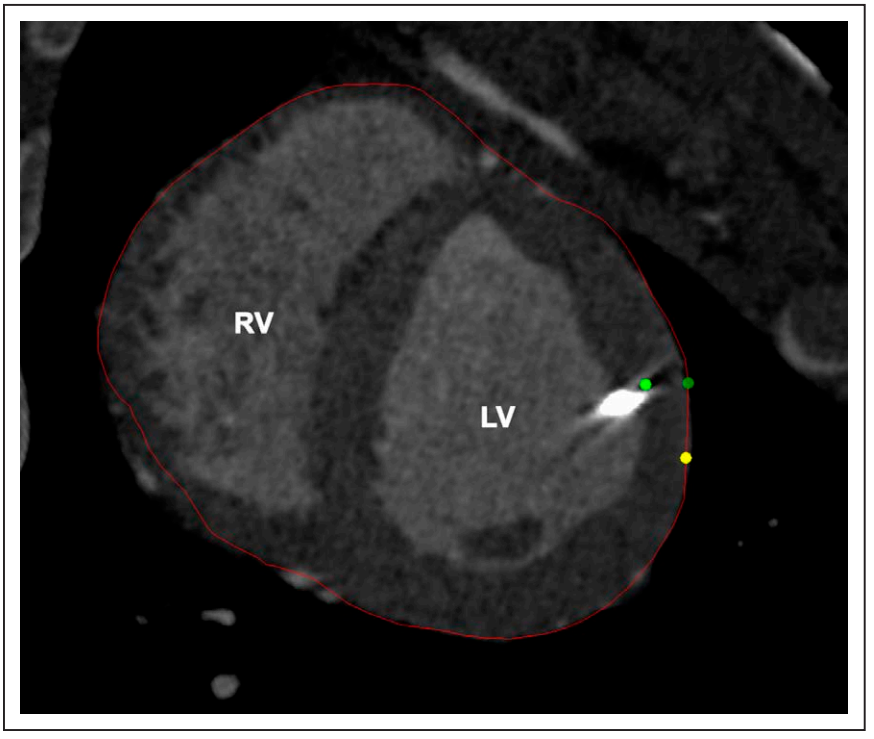

Figure 4. Representative example of the true pacing position (bright green), the electrocardiographic imaging (ECGi)-predicted location of earliest activation (yellow), and the pacing position projected onto the epicardial segmentation surface (darker green).
The red line shows the segmented epicardial surface. The high-density artifact close to the true pacing position is caused by one of the fiducial marker clips. LV indicates left ventricle; and RV, right ventricle.

been to establish the true location of earliest activation (ie, the pacing position) in the coordinate space of the ECGi map. Because the anatomy for the ECGi map is derived from a CT, any structures visible on the CT can be used as reference locations with high precision. Early attempts to validate ECGi, therefore, used patients with permanent or temporary electronic pacemakers. ECGi data were obtained in one subject with a cardiac resynchronization therapy device while pacing through the RV and LV leads and the point of earliest activation was compared with the lead tip locations on CT. Distances found in this patient were 7 mm for the RV pacing site and 11 mm for the LV pacing site.[19] In another study, paced activation from a permanent RV pacemaker lead (one patient) or temporary epicardial pacing post cardiac surgery (2 patients) was used as ground truth. Median ECGi accuracy in these 3 locations was found to be 15.8 mm.[20] In a third study ECGi located the pacing site in 3 patients with permanent RV pacing with a median distance of 24 mm.[21] More recent investigations used 3D electroanatomic mapping systems to determine the true pacing location. Relative to the registered 3D map, left atrium pacing locations were localized within 6.3±3.9 mm by the ECGi system in one report and epicardial LV pacing during ventricular tachycardia ablation was localized within 13±9 mm in another.[11,21] The most recent studies compared ECGi to invasive epicardial maps of sinus rhythm in patients with various conditions.[12,22] Distances between invasively mapped and ECGi-derived focal epicardial activation differed considerably in these studies: One investigation found a mean error of 13 mm while errors were 75 mm on average in the other.[12,22]

In contrast to pacing leads or radio-opaque fiducial markers, electroanatomic maps need to be registered to the CT/ECGi system first, introducing additional ambiguity. For the present study we, therefore, used fiducial markers to unambiguously establish the true pacing position on the ECGi map. Using this approach, our data confirms and expands the limited validation data which has been available previously.[19–21]

Factors Affecting Spatial Accuracy

Transmural and Intramural Spread of Activation

Localization of endocardial ventricular pacing sites might well pose the most challenging scenario for any ECGi system that reconstructs epicardial potentials. Early studies by Taccardi et al[18] showed that epicardial pacing results in a predictable epicardial activation pattern with an ellipse-shaped negativity centered on the pacing site and stretched along the direction of myocardial fibers. This central area of negative potential was surrounded by 2 positive maxima. Pacing at the endocardium or at shallow layers of the sub-endocardium, however, resulted in a less predictable pattern of epicardial activation in a canine model: Only 40% of endocardial pacing sites resulted in the above-mentioned epicardial pattern, with additional 20% leading to a well-defined positive potential maximum above the pacing site, and the remaining 40% exhibiting highly irregular patterns of epicardial activation.[18] These phenomena were later explained in an in silico analysis based on detailed anatomic data and were found to depend on the thickness of trabeculated myocardium at the pacing site.[23] More recently, the offset between intramural and subendocardial pacing sites and the earliest epicardial potential breakthrough was quantified in more detail in the canine heart and was observed to follow the oblique myocardial fiber orientation.[24] For pacing sites as little as 3 mm below the epicardium, the epicardial breakthrough no longer coincided with the pacing site but seems to be displaced along the myocardial fiber orientation.[24,25]

In the light of these challenges, a recent study investigating a different experimental ECGi system correlated the reconstructed epicardial potentials with true epicardial activation as measured by an epicardial electrode array.[10] Even in this setting, where the unknown transmural activation spread was taken out of the equation, a median localization error of 16 mm was observed.

It has been shown experimentally that the size of the virtual cathode increases with the pacing output, thus simultaneously exciting a larger volume of tissue at the time of pacing.[26] In theory, higher pacing outputs might therefore invalidate the assumption that the true site of earliest activation is located at the catheter tip. However, no correlation between pacing output and accuracy was found in our study.

Reconstruction on Epicardial Surface

The ECGi system calculates the inverse solution of electrocardiology on a user-defined epicardial surface. Therefore, the predicted locations of earliest activation will always be constrained to this surface, or, more specifically, to one of a finite number of discrete vertices defining this surface. Even if the inverse solution were exact, the earliest activation would still have only been observed at the surface vertex closest to the true pacing position. Therefore, the exact definition of the epicardial surface could theoretically limit the system's accuracy beyond the biophysical limitations outlined above. However, no significant difference in error distances was observed when using the nearest surface point instead of the real pacing location as reference location.

Volume Conductor Properties and Movement

Additional sources of error are due to properties of the thorax. Compared with torso tank experiments, where the heart is surrounded by uniformly conducting

saline, localization errors in vivo are consistently greater.[7,10,12,20,21] Inhomogeneous impedance and resistance across the different tissues and organs distort the body surface potentials when compared with the torso tank situation. Various smoothing techniques and modeling assumptions have been incorporated into ECGi algorithms to account for these thorax inhomogeneities.[27] Respiratory and cardiac movement add another layer of complexity. While the CT acquisition was performed in breath hold in our study, the pacing and ECGi waveform acquisition were not. Respiratory movement, therefore, induces a mismatch between the actual anatomy at the time of recording and the CT anatomy used for reconstruction. In theory, another mismatch could be found between heart geometry on the diastolic phase CT and the moving heart. However, the initial negative potentials analyzed in our study were seen during the initial depolarization phase (beginning of the paced P wave or the paced QRS complex). It has been shown in silico that a static diastolic geometry can be assumed during this phase without inducing additional errors in the inverse solution.[28]

Limitations

The results should be viewed in relation to the limitations inherent in this study. The true point of earliest activation was assumed to be at the catheter tip. Excitation by a pacing stimulus is complex, though, and the catheter tip location can only approximate the true 3D volume of myocardium being excited at the time of the stimulus.[26] With bipolar pacing, especially at pacing outputs near the diastolic threshold, excitation occurs preferentially as cathodal make excitation at the tip electrode.[29] However, we did not compare to unipolar stimulation in this study, and anodal excitation at the proximal electrode cannot be ruled out. Furthermore, we used focal activation to determine spatial accuracy. The performance of the system to reconstruct more complex activation patterns, such as scar-related reentry, is unknown, and further studies are warranted to elucidate this.

The electrode vest is designed for humans, and the electrode-skin interface has been optimized for human skin. Although we were able to fit the small or medium size vests to the pigs and obtain adequate recordings in most cases, impaired signal to noise ratio prevented the analysis in 4 locations and might have contributed to reduced accuracy. However, our approach to determine the pacing position with high precision using implanted fiducial markers as registration landmarks is only possible in a large animal model.

Most pacings were performed endocardially, while focal arrhythmias could originate from anywhere in the myocardium. Since the ECGi system reconstructs virtual electrograms on the epicardial surface, activation originating from the endocardium might be particularly challenging. Especially in the comparably thick-walled LV, fiber orientation, and anisotropic conduction might have added to the error between the endocardial pacing location and the reconstructed epicardial potential. However, error distances in the limited subset of epicardial pacing locations were not significantly different from those in endocardial pacing locations. Given the limited number of pacings per individual chamber, the study was possibly underpowered to detect small differences in precision between cardiac chambers.

Clinical Significance

It has previously been shown that the ECGi system is able to reliably detect the chamber of origin for focal arrhythmias.[2,3] This was confirmed in the present study. So far, noninvasive mapping has mostly been used clinically to identify an arrhythmogenic region of interest for the operator, which can then be mapped invasively in more detail before ablation. This approach has been shown to reduce procedure time and fluoroscopy dose with similar success rates.[30]

Completely noninvasive mapping and ablation workflows have recently been proposed using ECGi and different radiotherapeutic modalities.[31] The localization accuracy found in the present study should be considered when planning treatment targets based on ECGi data.

Conclusions

The ECGi system is able to determine the site of focal activation with a median error distance of 20.7 mm without significant differences in accuracy across cardiac chambers. It, therefore, seems well-suited to guide the catheter setup (left- or right-sided) and define a region of interest before invasive mapping and ablation, but the user should consider these limitations. Chamber identification is less accurate for septal foci since reconstruction of the potentials is limited to an epicardial surface.

ARTICLE INFORMATION

Received May 13, 2019; accepted September 24, 2019.

Correspondence

Douglas L. Packer, MD, Heart Rhythm Services, Mayo Clinic, St Marys Hospital, 1216 2nd St SW, AL 2-416, Rochester, MN 55902, Email packer@mayo.edu

Affiliations

Translational Interventional Electrophysiology Laboratory (S.H., M.E.R., H.K., S.W., A.S., K.H.M., K.D.P., L.K.N., D.L.P.) and Department of Radiology (G.J.M.), Mayo Clinic, Rochester, MN. Medtronic, Inc, Cleveland, OH (A.B.).

Sources of Funding

This study was funded by Medtronic Inc. Dr Hohmann is funded by the Deutsche Forschungsgemeinschaft (DFG, German Research Foundation)—project number 380200397. Dr Packer's work is funded in part by a clinician investigator award from the Mayo Foundation. His work is also supported by the Goldsmith Foundation as well as the Sanford Diller Foundation.

Disclosures

Dr Packer receives research funding from Abbott, Biosense Webster, Boston Scientific/EPT, CardioInsight, CardioFocus, Endosense, Hansen Medical, Medtronic, National Institutes of Health, Robertson Foundation, St Jude Medical, Siemens and Thermedical. He has provided consulting services for Abbott, Aperture Diagnostics, Biosense Webster, Inc., Biotronik, Boston Scientific, CardioFocus, Johnson & Johnson, MediaSphere Medical, Medtronic, St Jude Medical, Siemens, SigNum Preemptive Healthcare, Spectrum Dynamics, and Thermedical, receiving no personal compensation for these consulting activities. Mayo Clinic and Dr Packer have intellectual property in mapping technology which has been licensed to St Jude Medical, and Mayo Clinic and Dr Packer have received annual royalties. Dr Packer and Mayo Clinic jointly have equity in a privately held company, External Beam Ablation Medical Devices. A. Borenstein is an employee of Medtronic, Inc. The other authors report no conflicts.

REFERENCES

1. J Shah A, Hocini M, Pascale P, Roten L, Komatsu Y, Daly M, Ramoul K, Denis A, Derval N, Sacher F, Dubois R, Bokan R, Eliatou S, Strom M, Ramanathan C, Jais P, Ritter P, Haissaguerre M. Body surface electrocardiographic mapping for non-invasive identification of arrhythmic sources. *Arrhythm Electrophysiol Rev.* 2013;2:16–22. doi: 10.15420/aer.2013.2.1.16
2. Jamil-Copley S, Bokan R, Kojodjojo P, Qureshi N, Koa-Wing M, Hayat S, Kyriacou A, Sandler B, Sohaib A, Wright I, Davies DW, Whinnett Z, S Peters N, Kanagaratnam P, Lim PB. Noninvasive electrocardiographic mapping to guide ablation of outflow tract ventricular arrhythmias. *Heart Rhythm.* 2014;11:587–594. doi: 10.1016/j.hrthm.2014.01.013
3. Shah AJ, Hocini M, Xhaet O, Pascale P, Roten L, Wilton SB, Linton N, Scherr D, Miyazaki S, Jadidi AS, Liu X, Forclaz A, Nault I, Rivard L, Pedersen ME, Derval N, Sacher F, Knecht S, Jais P, Dubois R, Eliautou S, Bokan R, Strom M, Ramanathan C, Cakulev I, Sahadevan J, Lindsay B, Waldo AL, Haissaguerre M. Validation of novel 3-dimensional electrocardiographic mapping of atrial tachycardias by invasive mapping and ablation: a multicenter study. *J Am Coll Cardiol.* 2013;62:889–897. doi: 10.1016/j.jacc.2013.03.082
4. Hocini M, Shah AJ, Neumann T, Kuniss M, Erkapic D, Chaumeil A, Copley SJ, Lim PB, Kanagaratnam P, Denis A, Derval N, Dubois R, Cochet H, Jais P, Haissaguerre M. Focal arrhythmia ablation determined by high-resolution noninvasive maps: multicenter feasibility study. *J Cardiovasc Electrophysiol.* 2015;26:754–760. doi: 10.1111/jce.12700
5. Pullan AJ, Cheng LK, Nash MP, Ghodrati A, MacLeod R, Brooks DH. The inverse problem of electrocardiography. In: Macfarlane PW, van Oosterom A, Pahlm O, Kligfield P, Janse M, Camm J, editors. *Comprehensive Electrocardiology*. London: Springer London; 2010:299–344.
6. Messinger-Rapport BJ, Rudy Y. Noninvasive recovery of epicardial potentials in a realistic heart-torso geometry. Normal sinus rhythm. *Circ Res.* 1990;66:1023–1039. doi: 10.1161/01.res.66.4.1023
7. Oster HS, Taccardi B, Lux RL, Ershler PR, Rudy Y. Noninvasive electrocardiographic imaging: reconstruction of epicardial potentials, electrograms, and isochrones and localization of single and multiple electrocardiac events. *Circulation.* 1997;96:1012–1024. doi: 10.1161/01.cir.96.3.1012
8. Bear LR, Huntjens PR, Walton RD, Bernus O, Coronel R, Dubois R. Cardiac electrical dyssynchrony is accurately detected by noninvasive electrocardiographic imaging. *Heart Rhythm.* 2018;15:1058–1069. doi: 10.1016/j.hrthm.2018.02.024
9. Oosterhoff P, Meijborg VM, van Dam PM, van Dessel PF, Belterman CN, Streekstra GJ, de Bakker JM, Coronel R, Oostendorp TF. Experimental Validation of Noninvasive Epicardial and Endocardial Activation Imaging. *Circ Arrhythm Electrophysiol.* 2016;9:e004104. doi: 10.1161/CIRCEP.116.004104
10. Bear LR, LeGrice IJ, Sands GB, Lever NA, Loiselle DS, Paterson DJ, Cheng LK, Smaill BH. How accurate is inverse electrocardiographic mapping? A systematic in vivo evaluation. *Circ Arrhythm Electrophysiol.* 2018;11:e006108. doi: 10.1161/CIRCEP.117.006108
11. Cuculich PS, Wang Y, Lindsay BD, Faddis MN, Schuessler RB, Damiano RJ Jr, Li L, Rudy Y. Noninvasive characterization of epicardial activation in humans with diverse atrial fibrillation patterns. *Circulation.* 2010;122:1364–1372. doi: 10.1161/CIRCULATIONAHA.110.945709
12. Duchateau J, Sacher F, Pambrun T, Derval N, Chamorro-Servent J, Denis A, Ploux S, Hocini M, Jaïs P, Bernus O, et al. Performance and limitations of noninvasive cardiac activation mapping. *Heart Rhythm*. 2019;16:435–442. doi: 10.1016/j.hrthm.2018.10.010
13. National Research Council. *Guide for the Care and Use of Laboratory Animals*. Washington, DC: National Academies Press; 2011.
14. Hubrecht R, Kirkwood J, editors. *The UFAW Handbook on the Care and Management of Laboratory and Other Research Animals*. 8th ed. Oxford, UK: Wiley-Blackwell; 2010.
15. Okumura Y, Henz BD, Johnson SB, Bunch TJ, O'Brien CJ, Hodge DO, Altman A, Govari A, Packer DL. Three-dimensional ultrasound for image-guided mapping and intervention: methods, quantitative validation, and clinical feasibility of a novel multimodality image mapping system. *Circ Arrhythm Electrophysiol.* 2008;1:110–119. doi: 10.1161/CIRCEP.108.769935
16. Fedorov A, Beichel R, Kalpathy-Cramer J, Finet J, Fillion-Robin JC, Pujol S, Bauer C, Jennings D, Fennessy F, Sonka M, Buatti J, Aylward S, Miller JV, Pieper S, Kikinis R. 3D slicer as an image computing platform for the quantitative imaging network. *Magn Reson Imaging*. 2012;30:1323–1341. doi: 10.1016/j.mri.2012.05.001
17. Hintze JL, Nelson RD. Violin plots: a box plot-density trace synergism. *Am Stat*. 1998;52:181–184.
18. Taccardi B, Macchi E, Lux RL, Ershler PR, Spaggiari S, Baruffi S, Vyhmeister Y. Effect of myocardial fiber direction on epicardial potentials. *Circulation.* 1994;90:3076–3090. doi: 10.1161/01.cir.90.6.3076
19. Ramanathan C, Ghanem RN, Jia P, Ryu K, Rudy Y. Noninvasive electrocardiographic imaging for cardiac electrophysiology and arrhythmia. *Nat Med.* 2004;10:422–428. doi: 10.1038/nm1011
20. Ghanem RN, Jia P, Ramanathan C, Ryu K, Markowitz A, Rudy Y. Noninvasive electrocardiographic imaging (ECGI): comparison to intraoperative mapping in patients. *Heart Rhythm.* 2005;2:339–354. doi: 10.1016/j.hrthm.2004.12.022
21. Sapp JL, Dawoud F, Clements JC, Horácek BM. Inverse solution mapping of epicardial potentials: quantitative comparison with epicardial contact mapping. *Circ Arrhythm Electrophysiol.* 2012;5:1001–1009. doi: 10.1161/CIRCEP.111.970160
22. Graham AJ, Orini M, Zacur E, Dhillon G, Daw H, Srinivasan NT, Lane JD, Cambridge A, Garcia J, O'Reilly NJ, Whittaker-Axon S, Taggart P, Lowe M, Finlay M, Earley MJ, Chow A, Sporton S, Dhinoja M, Schilling RJ, Hunter RJ, Lambiase PD. Simultaneous comparison of electrocardiographic imaging and epicardial contact mapping in structural heart disease. *Circ Arrhythm Electrophysiol.* 2019;12:e007120. doi: 10.1161/CIRCEP.118.007120
23. Hren R, Nenonen J, Horácek BM. Simulated epicardial potential maps during paced activation reflect myocardial fibrous structure. *Ann Biomed Eng.* 1998;26:1022–1035. doi: 10.1114/1.73
24. Taccardi B, Punske BB, Macchi E, Macleod RS, Ershler PR. Epicardial and intramural excitation during ventricular pacing: effect of myocardial structure. *Am J Physiol Heart Circ Physiol.* 2008;294:H1753–H1766. doi: 10.1152/ajpheart.01400.2007
25. Anderson RH, Smerup M, Sanchez-Quintana D, Loukas M, Lunkenheimer PP. The three-dimensional arrangement of the myocytes in the ventricular walls. *Clin Anat.* 2009;22:64–76. doi: 10.1002/ca.20645
26. Wikswo JP Jr, Wisialowski TA, Altemeier WA, Balser JR, Kopelman HA, Roden DM. Virtual cathode effects during stimulation of cardiac muscle. Two-dimensional in vivo experiments. *Circ Res.* 1991;68:513–530. doi: 10.1161/01.res.68.2.513
27. Cheng LK, Bodley JM, Pullan AJ. Effects of experimental and modeling errors on electrocardiographic inverse formulations. *IEEE Trans Biomed Eng.* 2003;50:23–32. doi: 10.1109/TBME.2002.807325
28. Jiang M, Xia L, Shou G, Wei Q, Liu F, Crozier S. Effect of cardiac motion on solution of the electrocardiography inverse problem. *IEEE Trans Biomed Eng.* 2009;56:923–931. doi: 10.1109/TBME.2008.2005967
29. Dekker E. Direct current make and break thresholds for pacemaker electrodes on the canine ventricle. *Circ Res.* 1970;27:811–823. doi: 10.1161/01.res.27.5.811
30. Erkapic D, Greiss H, Pajitnev D, Zaltsberg S, Deubner N, Berkowitsch A, Möllman S, Sperzel J, Rolf A, Schmitt J, Hamm CW, Kuniss M, Neumann T. Clinical impact of a novel three-dimensional electrocardiographic imaging for non-invasive mapping of ventricular arrhythmias-a prospective randomized trial. *Europace.* 2015;17:591–597. doi: 10.1093/europace/euu282
31. Lehmann HI, Graeff C, Simoniello P, Constantinescu A, Takami M, Lugenbiel P, Richter D, Eichhorn A, Prall M, Kaderka R, Fiedler F, Helmbrecht S, Fournier C, Erbeldinger N, Rahm AK, Rivinius R, Thomas D, Katus HA, Johnson SB, Parker KD, Debus J, Asirvatham SJ, Bert C, Durante M, Packer DL. Feasibility study on cardiac arrhythmia ablation using high-energy heavy ion beams. *Sci Rep.* 2016;6:38895. doi: 10.1038/srep38895